eNeuro

Research Article: New Research
Neuronal Excitability

Divergent Changes in PBN Excitability in a Mouse Model of Neuropathic Pain

María L. Torruella-Suárez,[1] Benjamin Neugebauer,[1] Krystal Flores-Felix,[2] Asaf Keller,[2] Yarimar Carrasquillo,[1,3] and Nathan Cramer[2]

[1]National Center for Complementary and Integrative Health, National Institutes of Health, Bethesda, Maryland 20892, [2]Department of Neurobiology and UM-MIND, University of Maryland School of Medicine, Baltimore, Maryland 21201, and [3]National Institute on Drug Abuse, National Institutes of Health, Bethesda, Maryland 20892

Abstract

The transition from acute to chronic pain involves maladaptive plasticity in central nociceptive pathways. Growing evidence suggests that changes within the parabrachial nucleus (PBN), an important component of the spino–parabrachio–amygdaloid pain pathway, are key contributors to the development and maintenance of chronic pain. In animal models of chronic pain, PBN neurons become sensitive to normally innocuous stimuli and responses to noxious stimuli become amplified and more often produce afterdischarges that outlast the stimulus. Using ex vivo slice electrophysiology and two mouse models of neuropathic pain, sciatic cuff and chronic constriction of the infraorbital nerve (CCI-ION), we find that changes in the firing properties of PBN neurons and a shift in inhibitory synaptic transmission may underlie this phenomenon. Compared to PBN neurons from shams, a larger proportion of PBN neurons from mice with a sciatic cuff were spontaneously active at rest, and these same neurons showed increased excitability relative to shams. In contrast, quiescent PBN neurons from cuff mice were less excitable than those from shams. Despite an increase in excitability in a subset of PBN neurons, the presence of afterdischarges frequently observed in vivo were largely absent ex vivo in both injury models. However, $GABA_B$-mediated presynaptic inhibition of GABAergic terminals is enhanced in PBN neurons after CCI-ION. These data suggest that the amplified activity of PBN neurons observed in rodent models of chronic pain arise through a combination of changes in firing properties and network excitability.

Key words: afterdischarges; GABAB; intrinsic properties; sciatic; trigeminal

Significance Statement

Hyperactivity of neurons in the parabrachial nucleus (PBN) is causally linked to exaggerated pain behaviors in rodent models of chronic pain, but the underlying mechanisms remain unknown. Using two mouse models of neuropathic pain, we show the intrinsic properties of PBN neurons are largely unaltered following injury. However, subsets of PBN neurons become more excitable and $GABA_B$ receptor mediated suppression of inhibitory terminals is enhanced after injury. Thus, shifts in network excitability may be a contributing factor in injury-induced potentiation of PBN activity.

Received Oct. 16, 2023; revised Dec. 19, 2023; accepted Jan. 17, 2024.

The authors declare no conflict financial interests.

Author contributions: M.L.T-S., B.N., K.F-F., A.K., Y.C., and N.C. designed research; M.L.T-S., B.N., K.F-F., and N.C. performed research; A.K. and Y.C. contributed unpublished reagents/analytic tools; M.L.T-S., B.N., K.F-F., and N.C. analyzed data; M.L.T-S., A.K., Y.C., and N.C. wrote the paper.

This work was supported by the National Institutes of Health National Institute (NIH) of Neurological Disorders and Stroke Grants R01NS099245 (to A.K.), R01NS069568 (to A.K.), and R01NS127827 (to N.C.) and the Intramural Research Program at the NIH National Center for Complementary and Integrative Health (to Y.C.). The content is solely the responsibility of the authors and does not necessarily represent the official views of the National Institutes of Health. The funding sources had no role in study design; the collection, analysis and interpretation of data; the writing of the report; or in the decision to submit the article for publication.

Continued on next page.

Introduction

The parabrachial nucleus (PBN) is an important sensory processing and relay station for pain neurotransmission (Palmiter, 2018; Chiang et al., 2019). It is the main target of lamina I spinal nociceptive neurons (Cechetto et al., 1985; Bernard et al., 1989; Craig, 1995; Barik et al., 2018) and receives strong input from Tac1-expressing cells that transmit nociceptive information (Al-Khater and Todd, 2009; Chiang et al., 2020). Histological (Bellavance and Beitz, 1996; Hermanson and Blomqvist, 1996, 1997; Dutschmann and Herbert, 1997; Bester et al., 2000, 1997, Li et al., 2006; Jergova et al., 2008; Chiang et al., 2020;

Qi et al., 2022), electrophysiological (Bernard and Besson, 1990; Bernard et al., 1994; Bourgeais et al., 2001; Uddin et al., 2018), and calcium imaging studies (Campos et al., 2018; Barik et al., 2021), largely in rodents, established that PBN neurons respond to noxious stimulation in both naive and chronic pain conditions. PBN neurons become hyperresponsive in several models of chronic pain (Matsumoto et al., 1996; Uddin et al., 2018; Raver et al., 2020; Sun et al., 2020) and have increased spontaneous activity (Matsumoto et al., 1996; Raver et al., 2020). Afterdischarges, where PBN neurons remain active long after the noxious stimulus has ended, are also more prevalent in rodents with chronic pain (Uddin et al., 2018). Suppressing this enhanced excitability also suppresses chronic pain behaviors (Raver et al., 2020), suggesting changes in PBN excitability are causally linked to changes in pain perception.

Shifts in PBN excitability may arise from a combination of factors, including changes in the intrinsic properties of the neurons and changes in the strength of afferent inputs. Among the many neurotransmitters and neuromodulators in the PBN (Cramer et al., 2021; Teuchmann et al., 2022), GABA has emerged as a crucial locus of injury-induced plasticity. The central nucleus of the amygdala (CeA) sends GABAergic inputs to the PBN, which are attenuated in a model of chronic pain (Raver et al., 2020). Furthermore, optogenetic stimulation of this input can ameliorate pain-related behaviors (Raver et al., 2020; Hogri et al., 2022). The CeA is likely a source of tonic GABA to PBN in intact animals, as inhibition of part of this input is aversive even in the absence of injury (Torruella-Suárez et al., 2020). The PBN is under tonic suppression also by local GABAergic interneurons as optogenetic inhibition of this population can induce tactile hypersensitivity in otherwise pain-free animals (Sun et al., 2020). These studies position GABA as a key modulator of PBN activity in pain states.

While a wealth of literature has linked changes in PBN activity with chronic pain behaviors, the mechanisms driving these changes are largely unknown. In this study, we examined whether PBN hyperexcitability described in vivo is due to changes in intrinsic excitability and GABAergic signaling. As the previously described histological studies largely found differences in Fos expression in the lateral subnucleus of the PBN (lPBN), (Bellavance and Beitz, 1996; Hermanson and Blomqvist, 1996, 1997; Dutschmann and Herbert, 1997, Bester et al., 2000; Li et al., 2006; Jergova et al., 2008), the lPBN receives dense spinal inputs (Choi et al., 2020), and lPBN outputs have been linked to nocifensive behaviors (Chiang et al., 2020), we focused our recordings on this region. We further characterize passive and active membrane properties as well as spontaneous and evoked repetitive firing of PBN neurons, both at baseline and following nerve injury using two rodent models of neuropathic pain. Lastly, we tested the hypothesis that GABAergic input onto PBN neurons is subject to injury-induced plasticity. Our combined results demonstrate that lateral PBN neurons become more excitable following peripheral nerve injury and further suggest that enhancement of $GABA_B$-mediated presynaptic inhibition contributes to pain-related plasticity.

Materials and Methods

Subjects. All animal procedures were performed in accordance with the (author university) animal care committee's regulations. We used male and female C57BL/6J mice, but some experiments were performed only in male mice. These data are noted accordingly. All mice were bred in house or purchased from Jackson Laboratory and were 8–16 weeks old at the time of experimentation. Animals were group-housed prior to surgery in a reverse 12/12 light cycle with *ad libitum* food and water.

Correspondence should be addressed to Nathan Cramer at ncramer@som.umaryland.edu.

Sciatic cuff surgery. The sciatic cuff model of neuropathic pain was originally designed by Benbouzid et al. (2008). Male mice were anesthetized using isoflurane with an initial dose of 2% and a maintenance dose of 1% using a VetFlo anesthesia system (Kent Scientific). A hand warmer was used for warmth during the procedure and recovery. The right sciatic nerve was exposed, and a 2 mm piece of polyethylene tubing (0.38 mm ID/1.09 mm OD) was slid onto the nerve of cuff animals. The nerve was then returned to its original position, and wound clips were used to close the surgical site. Sham animals underwent the same process without cuff placement. Animals were placed in a new, clean cage and allowed to recover. Following surgery, mice were single- or pair-housed with a littermate that had received the same surgical intervention (sham or cuff) in a cage with a

perforated plexiglass divider. Animals were handled for a minimum of 5 d and then used 7–11 d after cuff/sham surgery. Due to the relatively early experimental endpoint wound clips were not removed. Immediately following slice preparation, the right sciatic nerve was exposed, and the experimenter confirmed the cuff placement.

Chronic constriction of the infraorbital nerve surgery. Male and female mice were anesthetized using a mixture of ketamine and xylazine (i.p.) and placed in a supine position on a temperature-controlled heating pad. Using aseptic surgical techniques, the right infraorbital branch of the trigeminal nerve was exposed through an intraoral incision and freed from surrounding connective tissue. Approximately 1–2 mm from its point of exit at the infraorbital foramen, the nerve was loosely ligated with sterile, 4-0 silk sutures. The incision was closed with Vetbond tissue adhesive, and the mice were monitored continuously until fully recovered from anesthesia. Daily postsurgical monitoring continued for 5–7 d while the mice continued to recover in their home cage.

von Frey testing. Sciatic cuff group: In a subset of animals, von Frey testing was performed 7 d after surgery as previously described (Torres-Rodriguez et al., 2023). Male mice were habituated in the von Frey apparatus in a red-lit room for 2 h prior to testing. The smallest filament that elicited a paw withdrawal response in at least three of five trials was taken as the mechanical threshold for each hindpaw. Tactile sensitivity was determined for both hindpaws by an experimenter blind to pain treatment.

CCI-ION group: We confirmed the presence of CCI-induced, mechanical allodynia in subset of mice (5 sham and 5 CCI-ION, male ∼10 weeks old) using a 1.4 g von Frey filament (Ugo Basile). Mice were gently held in the hand of the experimenter, and the filament was applied to the dorsal edge of the vibrissae pad ipsilateral to the ligated nerve. The number of nocifensive responses to five applications of the filament was recorded. Nocifensive responses were defined as the animal actively withdrawing its head or aggressively biting or swiping at the filament. We tested for differences in the fraction of nocifensive responses between groups at each time point (pre-surgery/baseline and again 1 and/or 2 weeks after surgery) using a mixed-effects model with Sidak's post hoc multiple-comparisons test.

Acute slice preparation. A laboratory from one institution performed recordings from the sciatic cuff model, whereas a laboratory from a second institution performed recordings from the CCI-ION model. We used similar recording protocols with the exceptions noted below. Sciatic cuff group: Mice were deeply anesthetized with 1.2 ml of intraperitoneal Avertin (1.25%). They were then transcardially perfused with approximately 30 ml of an ice-cold, choline-based, cutting solution (110.0 mM choline chloride, 25.0 mM $NaHCO_3$, 25 mM D-glucose, 12.7 mM L-ascorbic acid, 7.2 mM $MgCl_2$, 3.1 mM pyruvic acid, 2.5 mM KCl, 1.25 mM NaH_2PO_4, 0.5 mM $CaCl_2$). The brain was extracted, and 300 µm coronal slices were prepared using a Leica VT1200 S vibrating blade microtome (Leica Microsystems). Slices containing the right PBN were then transferred to a room temperature recovery chamber for at least 1 h prior to recording. The recovery chamber contained room temperature aCSF (125 mM NaCl, 25 mM D-glucose, 25 mM $NaHCO_3$, 2.5 mM KCl, 2 mM $CaCl_2$, 1.25 mM NaH_2PO_4, 1 mM $MgCl_2$). Both solutions were continuously perfused with a carbogen mixture (95%/5% O_2/CO_2).

CCI-ION group: Mice were anesthetized with a mixture of ketamine and xylazine and transcardially perfused with an ice-cold, NMDG-based, cutting solution containing the following (in mM): 92 NMDG, 30 $NaHCO_3$, 20 HEPES, 25 glucose, 5 Na-ascorbate, 2 thiourea, 1.25 NaH_2PO_4, 2.5 KCl, 3 Na-pyruvate, 0.5 $CaCl_2$, and 10 $MgSO_4$. Horizontal brain sections, 300 µm thick, from both left and right PBN were collected and used for recordings.

Whole-cell slice electrophysiology. Following recovery, slices were transferred to the recording chamber. Slices were continuously perfused (1–2 ml/min) with oxygenated aCSF. The recording chamber was maintained at 32–34°C using an inline solution heater and a heated platform under the control of a TC-344C Dual Channel Temperature Controller (sciatic cuff) or room temperature (CCI-ION). Neurons were identified using differential interference contrast on an Eclipse FN1 (Nikon) or BX-51 (Olympus) microscope. Freshly pulled glass micropipettes filled with a potassium methylsulfate/gluconate-based internal solution were used in all bridge-mode recordings: one lab containing (in mM) 120 CH_3KO_4S, 20 KCl, 14 phosphocreatine, 10 HEPES, 8 $NaCl_2$, 4 Mg-ATP, 0.3 Tris-GTP, and 0.2 EGTA. Another lab contained (in mM) 120 K-gluconate, 10 KCl, 10 HEPES, 1 $MgCl_2$, 0.5 EGTA, 2.5 Mg-ATP, and 0.2 Tris-GTP. For voltage-clamp recordings examining inhibitory currents, we used a high-chloride intracellular solution containing (in mM) 70 K-gluconate, 60 KCl, 10 HEPES, 1 $MgCl_2$, 0.5 EGTA, 2.5 Mg-ATP, and 0.2 GTP-Tris and included 50 µM APV and 20 µM CNQX in the recording aCSF. Signals were acquired using Axon MultiClamp 700B (Molecular Devices) and amplified using an Axon Digidata 1550 (Molecular Devices). Data were sampled at 100 kHz and low-pass filtered at 10 kHz.

Electrophysiological measurements. Capacitance and input resistance were calculated from a 25 ms ± 10 mV voltage step from −70 mV. Repetitive action potential firing was evoked using 500 ms depolarizing current steps of increasing magnitude (5 pA). This protocol was performed on both cells at their resting membrane potential (quiescent cells) and with additional current applied to maintain them at −70 mV (spontaneous cells). To minimize the impact of small changes in V_{rest}, we defined rheobase as the minimum current required to evoke an action potential in response to a depolarizing current step (500 ms) where the cell also fired to the next step.

Action potential analysis. In spontaneously firing neurons, the average action potential frequency was calculated from a 1 min period of stable firing without holding current. The Easy Electrophysiology software package (v2.5.0) was used to measure action potential kinetics (RRID: SCR_021190). The values from 20 action potentials were averaged for each cell. The voltage threshold was defined using a first derivative threshold of 33 mV/ms.

Paired-pulse ratios. All recordings of electrically evoked inhibitory postsynaptic currents (IPSCs) were performed in the presence of 20 μM CNQX and 50 μM APV to suppress AMPA and NMDA responses, respectively. IPSCs were evoked by passing current through a bipolar stimulating electrode at the edge of PBN. Stimulus intensities were determined for each cell by finding the lowest current threshold which reliably evoked an IPSC. Paired stimuli within a trial were 50 ms apart with 5–10 s between trials. Paired-pulse ratios were determined by averaging 10–20 individual trials and dividing the amplitude of the second response by the amplitude of the first response.

Statistics. Data are represented as mean ± 95% confidence interval (Figs. 1–5) or median ± 95% confidence interval (Figs. 6, 7). Repeated-measured two-way ANOVA, one-way ANOVA, mixed-effects analysis, chi-square, student's *t* tests, Mann–Whitney and Wilcoxon matched-pairs test were performed as appropriate using GraphPad Prism version 9.4.0 for Windows (GraphPad Software; www.graphpad.com). A single ROUT outlier late firing (LF) capacitance was removed from the dataset.

Results

Neuropathic injury model increases spontaneous activity in PBN neurons

To test the hypothesis that lPBN neurons are more excitable following injury, we used the sciatic cuff model of neuropathic pain (Benbouzid et al., 2008). Animals received either cuff implantation or sham surgery to the sciatic nerve 7–11 d prior to acute brain slice recordings (Fig. 1*A*). To validate that cuff implantation in the sciatic nerve induces tactile hypersensitivity, we performed the von Frey test 7 d after sciatic nerve surgery in a subset of animals. As expected, sham animals did not show hypersensitivity in the hindpaw ipsilateral to sciatic nerve surgery, compared with the contralateral hindpaw. In contrast, cuff animals presented hypersensitivity in the hindpaw ipsilateral to the sciatic cuff implantation, compared with the contralateral hindpaw (Fig. 1*B*; two-way ANOVA: interaction $F_{(1, 13)} = 54.03$, $p < 0.0001$; surgery group $F_{(1, 13)} = 31.23$, $p < 0.0001$; paw $F_{(1, 13)} = 84.25$, $p < 0.0001$; Bonferroni's multiple comparison: sham $p = 0.4$; cuff $p < 0.0001$).

Using whole-cell patch-clamp electrophysiology in acute brain slices, we found that a proportion of neurons fired spontaneously (i.e., in the absence of holding current) in the sham condition (22%, 13/60 cells). We have previously shown that PBN neurons can spontaneously fire in pain-free animals in vivo (Uddin et al., 2018). The proportion of spontaneously active neurons recorded in cuff animals (45%, 24/53 cells) was significantly higher (Fig. 1*C*; $\chi^2 = 6.726$, df = 1, $z = 2.597$, $p = 0.01$). We examined the intrinsic properties of these neurons and found no significant differences in capacitance (1D) or input resistance (1E). Resting membrane voltage (1F) and rheobase (1G) were also not significantly different between quiescent neurons from sham and cuff animals. To determine whether spontaneous neurons were located in any particular lPBN subnuclei, we mapped the location of the recording pipette following each recording (Fig. 1*H,I*). Spontaneous neurons were intermingled with quiescent neurons and recording locations were similar between sham and cuff groups. These data show that injury-induced increases in PBN spontaneous activity observed in vivo (Matsumoto et al., 1996; Raver et al., 2020) are preserved in an ex vivo acute brain slice preparation. Our results agree with findings suggesting that injury-induced PBN hyperexcitability may underlie pain hypersensitivity (Matsumoto et al., 1996; Uddin et al., 2018; Raver et al., 2020; Sun et al., 2020).

Spontaneous firing frequencies and action potential properties of individual neurons are unaltered in a neuropathic injury model

The increase in the number of spontaneously firing PBN neurons from cuff animals suggests that the intrinsic membrane properties, firing frequencies, or single-action potential waveforms of these neurons may be impacted by the cuff model (Fig. 2*A,B*). We re-examined the intrinsic properties shown in Figure 1, restricting our analysis to neurons that were firing spontaneously. The capacitance (Fig. 2*C*), input resistance (Fig. 2*D*), and average firing frequency (Fig. 2*E*) of spontaneously firing neurons were not significantly impacted by neuropathic injury. Examination of the single-action potential waveforms in these spontaneously active neurons showed that voltage threshold (Fig. 2*F*) and peak voltage (Fig. 2*G*) were not significantly different between groups. The rise time from voltage threshold to peak (Fig. 2*H*), decay from peak to 90% of threshold (Fig. 2*I*), and action potential width (Fig. 2*J*) were not significantly different between sham and cuff groups. These results demonstrate that, while the number of spontaneously firing PBN neurons increases following neuropathic injury, this effect does not arise from changes in intrinsic properties or action potential kinetics.

Firing properties of PBN neurons are heterogeneous

We next examined the firing properties evoked by a prolonged (500 ms) depolarizing current step. We distinguished four firing types: spontaneous firing, regular spiking (RS), LF, and reluctant firing (Fig. 3*A*). Neurons that fired an action potential

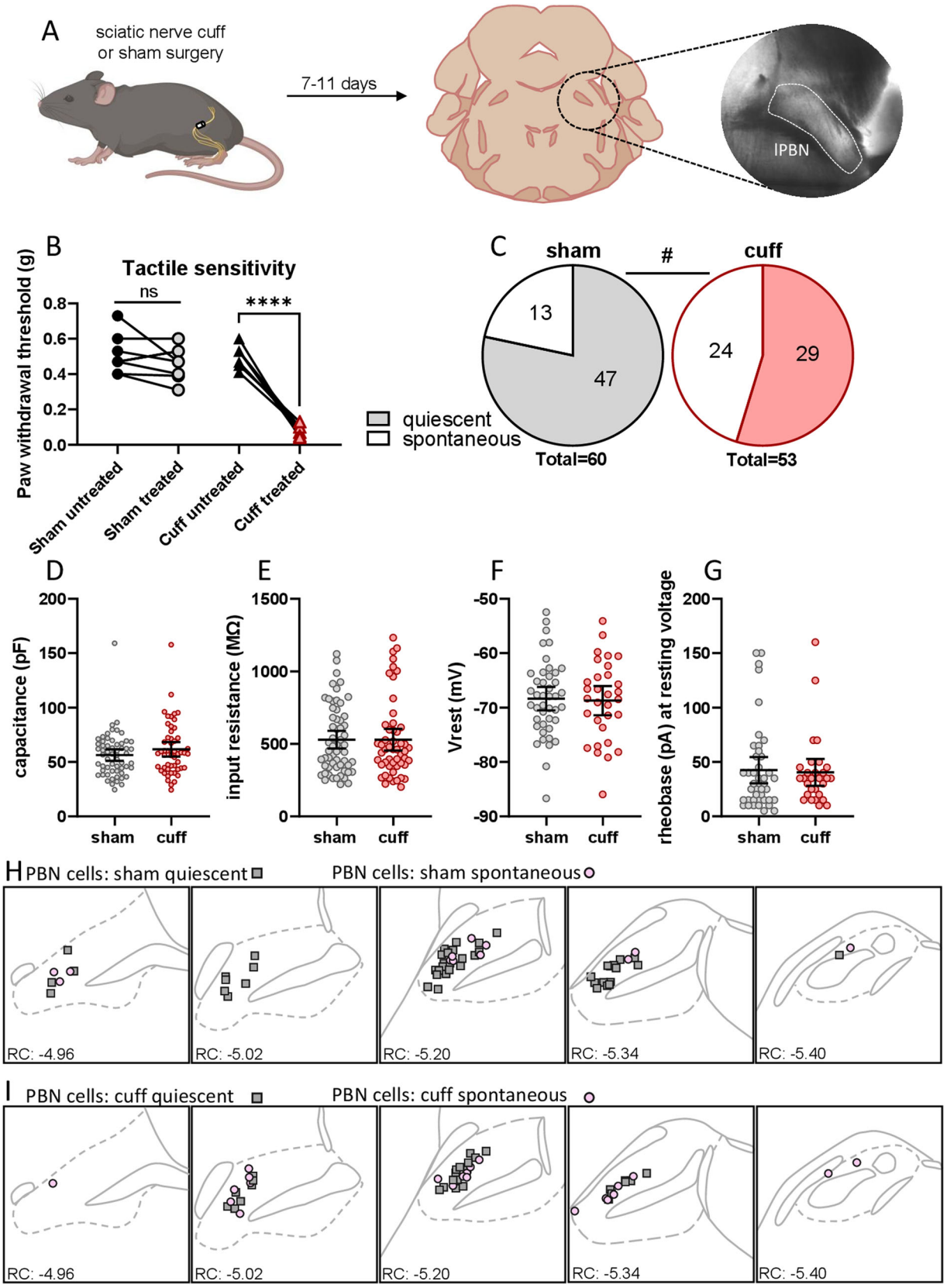

Figure 1. Continued.

within 30 ms of the beginning of the current step were classified as RS (27%, 16/60 sham cells), and those that fired after that point were classified as LF (42%, 25/60 sham cells). Both RS and LF neurons fired repetitively without much variation in interspike interval throughout the series of steps. Neurons that did not fire in response to the 80 pA depolarizing current injection, but fired at higher current injection steps, were classified as reluctant (8%, 5/60 sham cells). When spontaneously firing neurons were held at −70 mV, they also largely fell within these categories. Five neurons did not fall into any of these categories and were excluded from further analysis (Fig. 3*B*). Two neurons presented burst-like firing at low current steps, and three neurons showed strong depolarizing blocks.

To evaluate the excitability of each firing type, we analyzed their evoked firing in response to a series of prolonged (500 ms) depolarizing current steps. Both RS and LF neurons fired an increased number of spikes as a function of the amplitude of depolarizing current injections (Fig. 3*C*). In contrast, reluctant neurons rarely fired within the amplitude steps shown here. Quantification of the input–frequency relationship between firing types showed that RS neurons were the most excitable and reluctant neurons the least (mixed-effects analysis: current step $F_{(1.498,\ 56.83)} = 68.09$; firing type $F_{(2,\ 38)} = 37.39$; interaction $F_{(40,\ 759)} = 23.28$; all $p < 0.05$). The differences in excitability between firing types were also reflected in the rheobase (Fig. 3*D*; one-way ANOVA: $F_{(2,\ 40)} = 122.0$, $p < 0.0001$; all pairwise-comparisons $p < 0.0001$), with RS neurons showing the lowest rheobase and reluctant the highest.

Intrinsic membrane properties can dictate firing patterns and strongly influence neuronal output. To gain insight into the mechanisms underlying these heterogeneous firing patterns, we examined the intrinsic properties of each firing type. PBN neurons with different firing types had significantly different capacitances (Fig. 3*E*; one-way ANOVA: $F_{(3,\ 53)} = 6.815$, $p = 0.0006$), input resistances (Fig. 3*F*; one-way ANOVA: $F_{(3,\ 54)} = 4.508$, $p = 0.007$), and resting membrane potentials (Fig. 3*G*; one-way ANOVA: $F_{(2,\ 40)} = 9.263$, $p = 0.0005$). Post hoc analyses further revealed that reluctant neurons have significantly higher capacitance values than spontaneous and RS neurons (Bonferri-corrected post hoc vs spont $p = 0.04$, vs RS $p = 0.01$), as did LF neurons (vs spont $p = 0.0398$, vs RS $p = 0.0096$). Reluctant neurons also had the lowest average input resistance of all firing types (vs spont $p = 0.04$; vs RS $p = 0.04$) and the most hyperpolarized average resting membrane potential. Lastly, resting membrane potential in RS neurons was significantly more depolarized than either LF or reluctant cells (vs LF $p = 0.002$; vs reluctant $p = 0.004$). Taken together, these data demonstrate that the lPBN is composed of cells with different firing types that have different intrinsic membrane properties and firing responses to depolarizing current injections.

Neuropathic injury model bidirectionally impacts evoked firing

As most neurons fell into the RS or LF categories, we focused on those populations in evaluating the effects of neuropathic injury on intrinsic membrane properties and excitability. In RS and LF neurons, there was no difference in capacitance or input resistance between cuff and sham groups (Table 1). We next examined evoked firing in response to prolonged depolarizing current injections, as we hypothesized that the increased responsivity to sensory stimuli described in vivo (Matsumoto et al., 1996; Uddin et al., 2018; Raver et al., 2020) would translate as a magnified response to depolarizing current injection. Notably, RS neurons from cuff animals fired *fewer* APs than those from sham animals (Fig. 4*A*,*B*; mixed-effects analysis: current step $F_{(1.567,\ 29.46)} = 86.22$, $p < 0.0001$; surgery $F_{(1,\ 19)} = 8.090$, $p = 0.01$; interaction $F_{(20,\ 376)} = 3.903$, $p < 0.0001$) without a concurrent increase in rheobase (Fig. 4*C*; $p = 0.1221$). This hypoexcitability was not due to a difference in resting membrane potential, as the resting membrane voltage was not significantly different between conditions (Fig. 4*D*; $p = 0.3010$). In LF neurons, however, there were no significant differences in evoked firing frequencies (Fig. 4*E*), rheobases (Fig. 4*F*), or resting membrane potentials (Fig. 4*G*). These data suggest that, contrary to our hypothesis, injury reduces evoked excitability in a subset of PBN neurons.

To examine the evoked firing properties of spontaneously firing neurons, we held them at −70 mV and applied prolonged depolarizing current steps to elicit firing (Fig. 4*H*). Spontaneous neurons from sham animals held at −70 mV were classified as RS and LF neurons based on their firing responses to depolarizing current injections. Cuff treatment did not measurably impact capacitance or input resistance for either spontaneous RS or spontaneous LF neurons (Table 1). In contrast to the quiescent neurons, the spontaneous RS neurons from cuff animals had *higher* evoked excitability, compared with those from sham (Fig. 4*I*; mixed-effects analysis: current step, $F_{(1.930,\ 16.69)} = 93.19$, $p < 0.0001$; treatment, $F_{(1,\ 9)} = 5.974$, $p = 0.04$; interaction, $F_{(20,\ 173)} = 3.468$, $p < 0.0001$.) There was no significant change in rheobase (Fig. 4*J*) in these neurons held at −70 mV (Fig. 4*K*). There was no difference in the evoked excitability (Fig. 4*L*) or rheobase (Fig. 4*M*) of spontaneous LF neurons held at −70 mV (Fig. 4*N*). Taken together, these data show that there are divergent changes in injury-induced excitability in a subset of PBN neurons with higher excitability observed in one population (spontaneous RS) and lower excitability in a second (quiescent RS).

←

Figure 1. Neuropathic injury model increases spontaneous activity in PBN neurons. ***A***, Mice were used 7–11 d after sciatic cuff surgery for slice electrophysiology in pBN. ***B***, Cuff surgery induced tactile hypersensitivity, but sham surgery had no effect. ***C***, Proportion of spontaneously firing neurons in each firing category from sham (22%, 13/60) and cuff (45%, 24/53) animals. Neuronal properties, including (***D***) capacitance, (***E***) input resistance, (***F***) resting membrane potential, (***G***) and rheobase, were similar in sham and cuff animals. Anatomical location of the recorded neurons from (***H***) sham and (***I***) cuff animals. Gray squares: quiescent cells. Pink circles: spontaneously firing cells. Bonferroni corrected *t* test: $^{****}p < 0.0001$. χ^2 test: $^{\#}p < 0.05$.

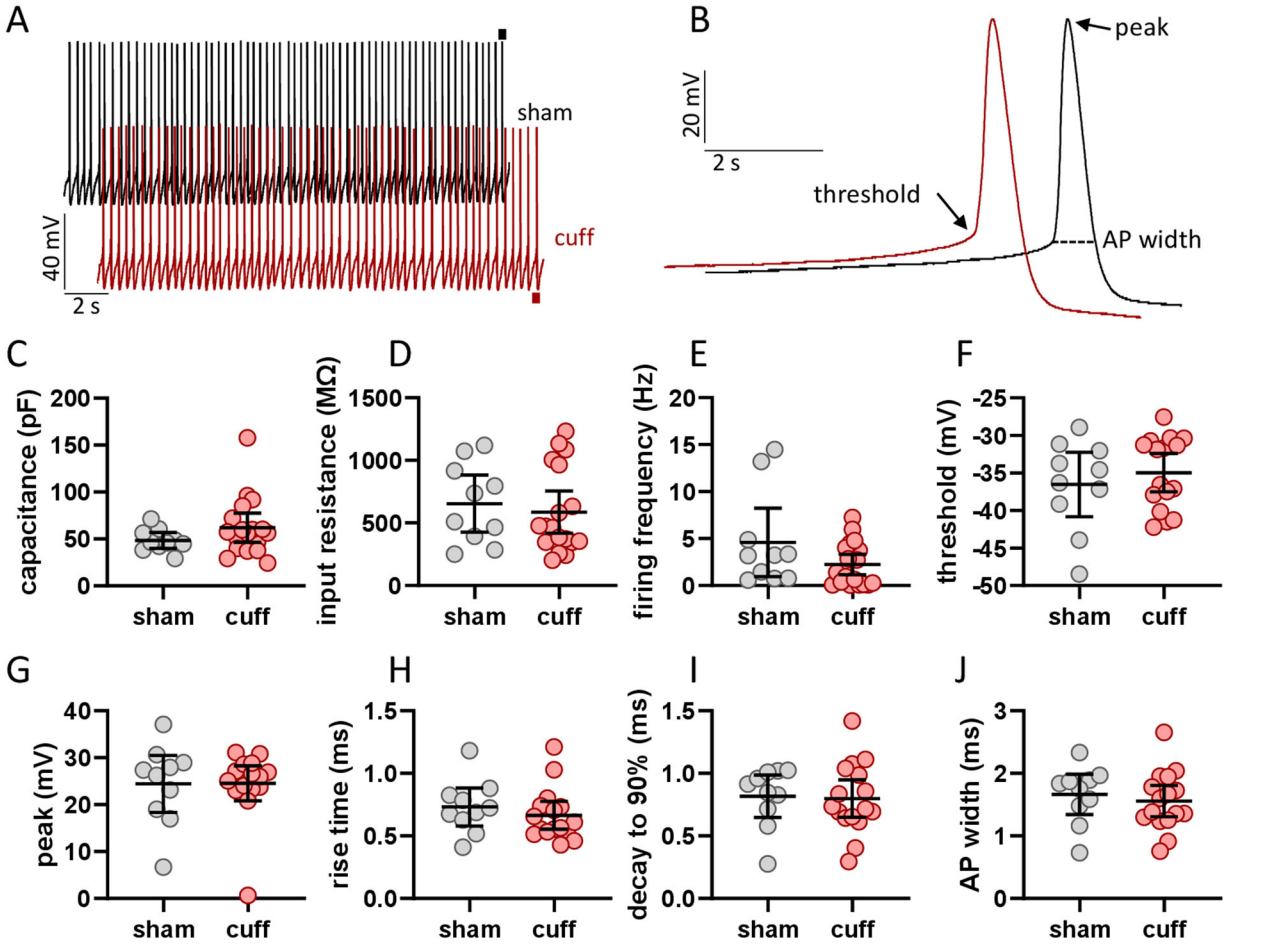

Figure 2. Spontaneous firing frequencies and action potential properties are unaltered in a neuropathic injury model. ***A***, Example traces of spontaneous firing in neurons from sham (black) and cuff (magenta) animals. ***B***, Example action potentials from panel ***A*** indicated by horizontal bars. There were no differences between neurons from sham and cuff cells in (***C***) capacitance, (***D***) input resistance, (***E***) firing frequency, (***F***) action potential threshold, (***G***) peak, (***H***) rise time from threshold to peak, (***I***) decay from peak to 90% of threshold, or (***J***) total action potential width.

Parabrachial after discharges ex vivo do not arise from changes in intrinsic properties of PBN neurons

In addition to enhanced responses to noxious stimulation, PBN neurons recorded in chronic pain models in vivo often continue firing at elevated levels long after the stimulus has ended (Uddin et al., 2018; Raver et al., 2020). Similar to the changes in evoked excitability described above, these afterdischarges may contribute to the exaggerated pain behaviors observed in these models. In a second series of experiments, using the chronic constriction injury of the infraorbital nerve (CCI-ION) model of neuropathic pain, we sought to determine whether afterdischarges are intrinsic to PBN neurons or arise from extrinsic factors, such as alterations in synaptic strength. We chose to use CCI-ION instead of sciatic nerve cuff for these experiments to help isolate mechanisms of PBN excitability that could be common to neuropathic pain in general rather than specific to certain models. We used whole-cell patch-clamp techniques to test the prediction that afterdischarges are more prevalent in PBN neurons from injured mice (Fig. 5*A*). These recordings were performed in a different laboratory than those focused on the intrinsic properties described above but using similar ex vivo techniques. Differences in the recording conditions are described in the Materials and Methods.

Similar to the tactile hypersensitivity observed in mice with a sciatic nerve cuff, male and female mice with a CCI-ION developed mechanical allodynia in the vibrissae pad innervated by the ligated nerve (Fig. 5*B*). When measured 1–2 weeks after injury, mice of both sexes in the CCI-ION group showed a higher frequency of nocifensive responses to five normally innocuous mechanical stimuli applied to the vibrissa pad relative to shams (mixed-effects model with Sidak's correction for post hoc multiple comparisons, $p < 0.0001$ at 1–2 weeks, $n = 5$ per group).

We recorded from a total of 23 neurons (sham, $n = 12$ neurons from 1 male and 3 female mice; CCI-ION, $n = 11$ neurons from 4 female mice), all of which displayed one of the firing patterns described above. Most were RS ($n = 8$ sham and 7 CCI), and the remaining were either LF ($n = 1$ sham and 4 CCI) or fast spiking (FS, $n = 3$ sham). Our lower sample size in this model prevents the statistical comparison of intrinsic properties. However, spontaneous firing was present in 6 of 12 neurons from sham mice (50%) and 4 of 11 neurons from CCI mice (36%). In quiescent cells, the median resting

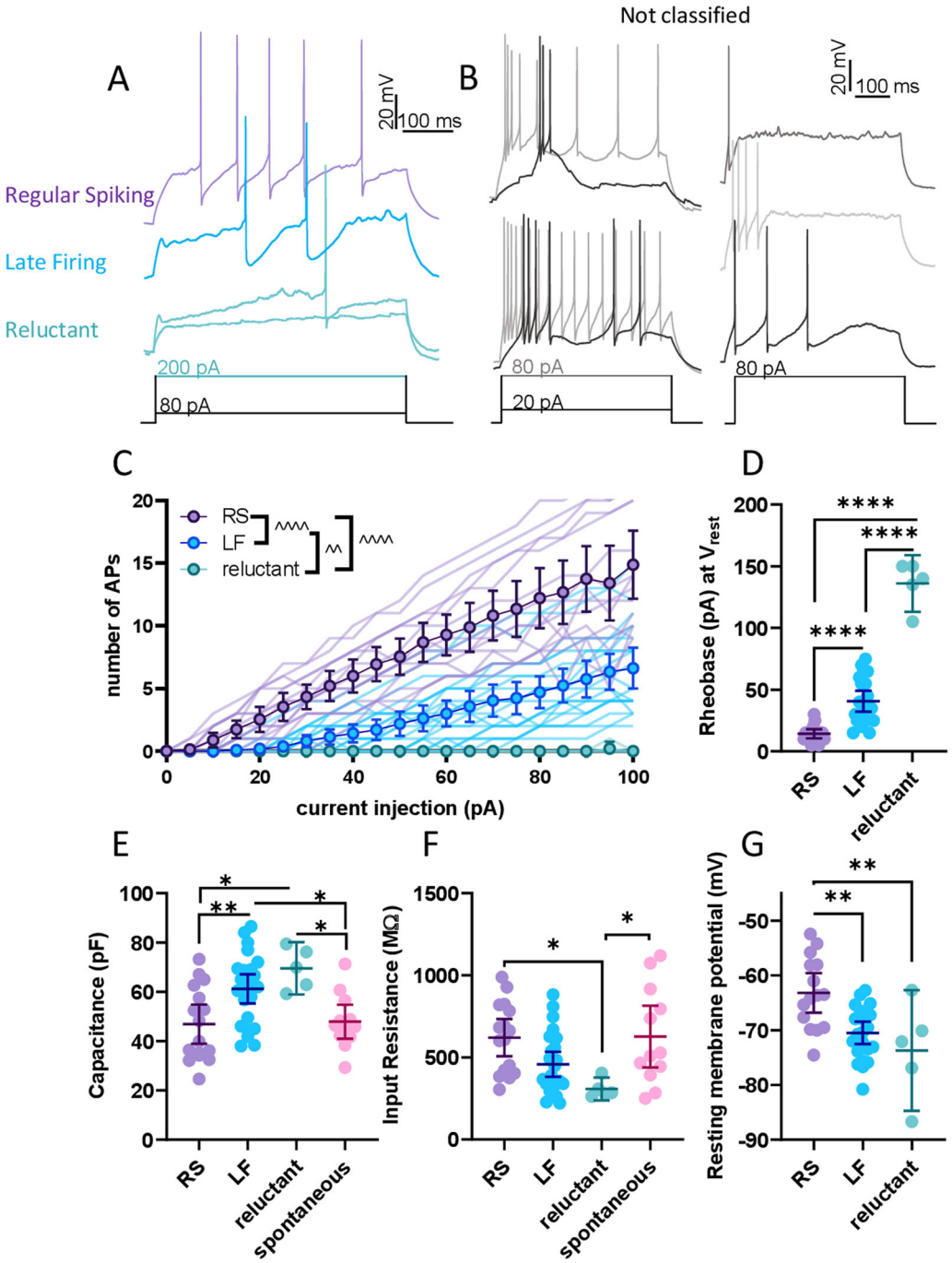

Figure 3. Heterogeneous firing types of PBN neurons. ***A***, Representative traces of RS, LF, and reluctant neurons. ***B***, Representative traces of neurons that did not fit the main firing types. ***C***, Input–frequency and (***D***) rheobase for each firing type. Intrinsic properties, including (***E***) capacitance, (***F***) input resistance, and (***G***) resting membrane potential were all different between firing types. Data for spontaneous neurons are replicated from Figure 2 for comparison. Each datapoint represents a cell. Bonferroni corrected *t* test: $^{*}p<0.05$, $^{**}p<0.01$, $^{****}p<0.0001$. Main effect from mixed-effects analysis: $^{\wedge\wedge}p<0.01$, $^{\wedge\wedge\wedge\wedge}p<0.0001$.

membrane potential of sham neurons was −58 mV ($n=6$; 95% CI: −67 to −49 mV) and −57 mV in neurons from CCI mice ($n=5$, 95% CI: −59 to −49 mV).

We used a variety of depolarizing current pulses that varied in shape and duration as a surrogate for synaptic input, in an attempt to evoke afterdischarges. These protocols included sinusoidal pulses of variable frequency (0.5–10 Hz) and amplitude, square pulses of fixed duration (0.5 or 1 s) but increasing intensity (2–3 times the rheobase), and square pulses of fixed intensity but increasing duration (0.25–5 s). The pie chart in Figure 5C shows the number of cells in which each protocol was used in an attempt to generate afterdischarges. Some cells were tested with multiple protocols.

Table 1. Intrinsic properties of quiescent and spontaneously active PBN neurons

	Quiescent				Spontaneous			
	RS		LF		RS		LF	
	Sham	Cuff	Sham	Cuff	Sham	Cuff	Sham	Cuff
Capacitance (pF)	46.85 ± 14.94 (*n* = 16)	55.4 ± 21.08 (*n* = 7)	65.11 ± 23.91 (*n* = 25)	59.84 ± 15.89 (*n* = 18)	46.44 ± 12.59 (*n* = 7)	50.21 ± 23.54 (*n* = 6)	50.05 ± 10.32 (*n* = 4)	59.72 ± 25.83 (*n* = 11)
R_{in} (MΩ)	620.6 ± 212.8 (*n* = 16)	481.7 ± 170.8 (*n* = 7)	458.0 ± 184.0 (*n* = 25)	551.6 ± 264.0 (*n* = 18)	581.8 ± 298.5 (*n* = 7)	563.3 ± 307.5 (*n* = 6)	734.1 ± 344.0 (*n* = 4)	590.7 ± 302.0 (*n* = 11)
Rheobase at native V_{rest} (pA)	14.33 ± 7.76 (*n* = 15)	20.83 ± 9.704 (*n* = 6)	40.71 ± 18.59 (*n* = 21)	37.65 ± 15.12 (*n* = 17)	NA	NA	NA	NA
Rheobase at −70 mv (pA)	33.08 ± 20.37 (*n* = 13)	50.0 ± 42.43 (*n* = 7)	42.37 ± 29.46 (*n* = 19)	40.88 ± 18.31 (*n* = 17)	25.00 ± 7.071 (*n* = 6)	21.67 ± 5.164 (*n* = 6)	46.25 ± 22.50 (*n* = 4)	34.00 ± 20.39 (*n* = 10)

NA, not applicable.

Representative recordings of each protocol are shown in Figure 5*D–F*, respectively. Regardless of the parameters, the occurrence of afterdischarges following any form of depolarizing current pulse was rare and observed in only 2 of 23 PBN neurons, both of which were RS neurons from CCI mice. Even in these two cells, afterdischarges occurred irregularly. For example, the cell in Figure 5*F* produced an afterdischarges following the first depolarizing pulse but failed to do so on subsequent depolarizations. These results suggest that the enhanced excitability and responsiveness of PBN neurons observed in chronic pain models in vivo are unlikely to arise from changes in intrinsic properties of the PBN neurons.

$GABA_B$-mediated presynaptic inhibition is enhanced in PBN neurons in a neuropathic injury model

An alternative mechanism for the generation of afterdischarges is a shift in the balance of excitation and inhibition within PBN. Indeed, chronic pain behaviors in mice and rats with a CCI-ION injury are causally related to diminished inhibitory drive from the CeA (Raver et al., 2020). Inhibitory afferents in PBN are regulated by several classes of presynaptic receptors (Cramer et al., 2021; Teuchmann et al., 2022), with particularly strong and consistent modulation arising from $GABA_B$ receptors (Cramer et al., 2021).

We investigated the potential contribution of $GABA_B$ receptors in injury-induced changes in PBN excitability by measuring the amplitude of pharmacologically isolated, evoked inhibitory postsynaptic currents (eIPSC) in PBN neurons (Fig. 6*A*). We placed a bipolar stimulating electrode at the edge of PBN of acute brain slices and recorded neuronal responses to paired-pulse stimulation in 13 neurons from 7 sham mice (2 female and 5 male) and 20 neurons from 11 CCI mice (4 female and 7 male). The mean amplitude of the second response divided by the mean amplitude of the first response is called the PPR and changes in this metric reflect changes in synaptic release probability (Kim and Alger, 2001; Sanabria et al., 2004). As shown in Figure 6*B*, electrical stimulation within PB reliably produced IPSCs in neurons from both sham and CCI mice. Quantification of the first eIPSC amplitude (Fig. 6*C*) and PPR (Fig. 6*D*) revealed no differences between the two experimental groups (PPR: sham = 1.2, 1.0–1.5, CCI = 1.1, 1.0–1.4; mean with 95% CI, unpaired *t* test, $p = 0.9$).

We hypothesized that the level of tonic GABA release ex vivo may be insufficient to activate presynaptic $GABA_B$ receptors and, consequently, any changes in the strength of this pathway may not be observable under these baseline recording conditions. To address this possibility, we measured eIPSC PPR before and after bath application of either a $GABA_B$ agonist (1 μM baclofen) or antagonist (1–5 μM CGP-55845; Fig. 6*E*). As shown in the example recordings and group data in Figure 6*F*, baclofen did not alter eIPSC PPR in PBN neurons from sham mice (baseline, 1.2, 0.8–2; baclofen, 0.9, 0.7–1.3; Wilcoxon matched-pairs test: $p = 0.2$, $n = 6$). However, the median eIPSC PPR in neurons from CCI mice was significantly increased by baclofen application (baseline, 1.0, 0.8–1.2 95% CI; baclofen, 1.6, 1.2–1.8 95% CI; Wilcoxon matched-pairs test, $p = 0.03$, $n = 6$). In contrast, the $GABA_B$ receptor antagonist CGP-55845 had no effect on eIPSC PPR in neurons from either sham (baseline, 1.2, 0.9–1.4; CGP: 1.4, 1.0–1.8; Wilcoxon matched-pairs test, $p = 0.16$, $n = 7$) or CCI mice (baseline, 1.4, 1.1–1.6; CGP, 1.3, 1.0–1.6; Wilcoxon matched-pairs test, $p = 0.2$, $n = 14$, Fig. 6*G*).

Together, these results indicate that, ex vivo, there are no differences in tonic $GABA_B$ receptor–mediated suppression of inhibitory synapses in PBN following CCI. However, when activity in GABAergic afferents increases, feedback inhibition at these synapses becomes stronger in mice with CCI. This increase in $GABA_B$ receptor–mediated suppression at inhibitory terminals may enable the exaggerated responses to noxious stimuli and subsequent afterdischarges commonly observed this chronic pain model in vivo.

Discussion

We investigated mechanisms of injury-induced PBN hyperexcitability using an ex vivo acute brain slice preparation. The percent of spontaneously firing neurons was higher in the cuff model of neuropathic pain, in line with in vivo studies demonstrating an increase in spontaneous activity in the PBN in pain. We found extensive electrophysiological heterogeneity within the lPBN of both sham and injured mice, including neurons with RS, FS, and reluctant firing patterns. Although

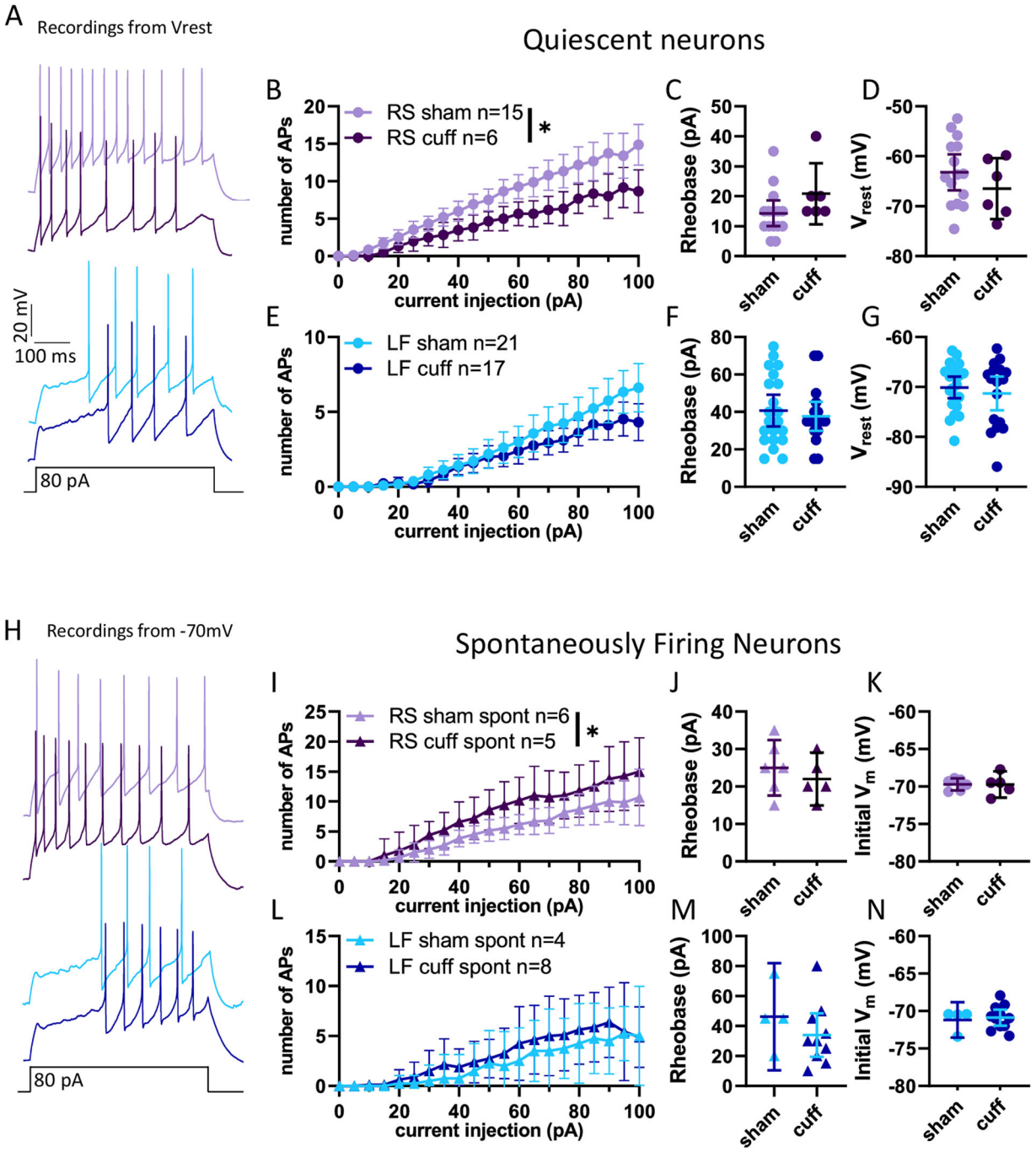

Figure 4. Neuropathic injury model bidirectionally impacts evoked firing. ***A***, Representative traces of action potentials in RS and LF neurons from sham and cuff animals. ***B***, Quiescent RS neurons were more excitable in sham animals than cuff animals, though (***C***) rheobase and (***D***) resting membrane potential were not different. ***E***, Quiescent LF neurons were not impacted by neuropathic injury in either repetitive firing (***F***) rheobase or (***G***) resting membrane potential. ***H***, Representative traces of spontaneous firing in RS and LF neurons from sham and cuff animals. ***I***, Input–frequency relationship for RS neurons held at −70 mV. ***J***, Rheobase and initial membrane voltage (***K***) spontaneous RS neurons. ***L***, Input–frequency relationship for LF neurons held at −70 mV. ***M***, Rheobase and initial membrane voltage (***N***) spontaneous LF neurons. Data for sham neurons are replicated from Figure 3 for comparison. Main effect from mixed-effects analysis: $^{*}p < 0.05$.

there were no differences in the intrinsic properties within the subclasses of PBN neurons, spontaneously active RS neurons from mice with a cuff injury were more excitable compared with shams. In addition, $GABA_B$-mediated presynaptic inhibition of inhibitory synapses in PBN was enhanced following nerve injury. These results suggest that increased excitability of PBN neurons, and suppression of inhibitory afferent inputs, contributes to PBN hyperexcitability and increased pain behaviors in rodent models of chronic pain.

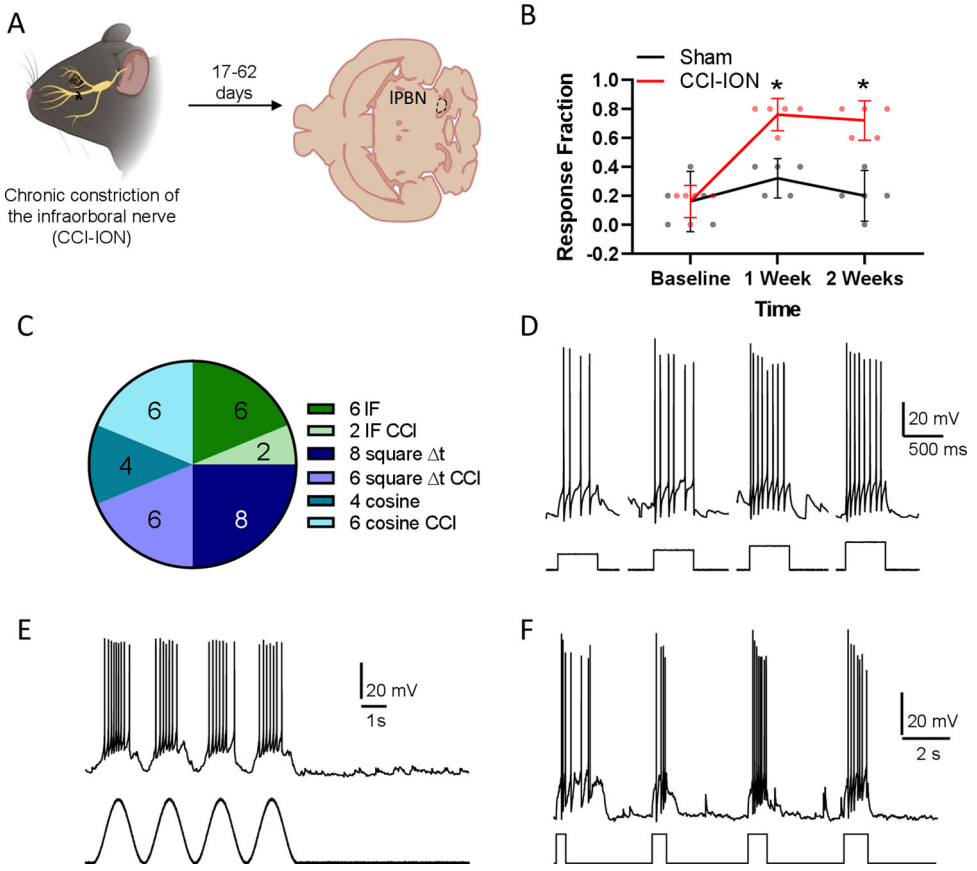

Figure 5. After discharges do not reflect intrinsic membrane properties of PBN neurons. ***A***, Experimental design for investigating afterdischarges. CCI-ION was used as a model for peripheral nerve injury and electrophysiological data were acquired from horizontal sections through the PBN. ***B***, CCI-ION results in mechanical hypersensitivity in both sexes that persisted for at least 2 weeks after injury (***C***). Summary of the number of neurons from sham and CCI mice tested with different current injection protocols in attempts to evoke afterdischarges. We recorded from a total of 12 neurons from sham and 11 neurons from CCI mice, but some PBN neurons were tested with multiple protocols. Examples of each protocol include square pulses of fixed duration and increasing magnitude (***D***), depolarizing sinusoidal currents (***E***), and square pulses of fixed intensity and increasing duration (***F***). Afterdischarges, such as the one following the first depolarizing square pulse in ***F***, were rarely observed and could not be consistently evoked, in any PBN neuron. Mixed-effects analysis with Sidak's multiple-comparisons test, $^{*}p < 0.05$.

Neuronal heterogeneity in the PBN

Neurons in the PBN displayed significant heterogeneity in their intrinsic properties and firing patterns. Electrophysiological heterogeneity has been described previously in the lPBN, although this work has largely focused on general differences between neurons from different PBN subnuclei (Kobashi and Bradley, 1998; Hayward and Felder, 1999). Similar heterogeneity exists in gene expression, function, input targets, and output populations in the PBN (Bernard and Besson, 1990; Bernard et al., 1994; Uddin et al., 2018; Chiang et al., 2020; Yang et al., 2021; Karthik et al., 2022; Pauli et al., 2022). Although the relationships between these different functional, genetic, and anatomical properties are just beginning to be uncovered (Pauli et al., 2022), our observation that nerve injury alters the excitability of just a subset of PBN neurons suggests these factors contribute to PBN plasticity in chronic pain conditions.

Preservation of injury-induced hyperexcitability the PBN slices

Among its many functions (Campos et al., 2018; Palmiter, 2018; Nagase et al., 2019), the PBN plays a crucial role in nociceptive and nocifensive behaviors. In response to injury, PBN neurons in vivo increase their spontaneous activity (Matsumoto et al., 1996; Raver et al., 2020), as well as their evoked responses (Matsumoto et al., 1996; Uddin et al., 2018; Raver et al., 2020). We find similar injury-induced changes in PBN spontaneous activity and, in a subset of neurons, enhanced excitability ex vivo, and add the novel finding that RS neurons are particularly impacted after nerve injury.

Divergent changes in evoked excitability

Neuropathic injury-induced divergent changes in the evoked excitability of RS PBN neurons (Fig. 4). We hypothesized that PBN neurons would become hyperexcitable following injury. Consistent with this hypothesis, spontaneously firing neurons were more excitable in injured mice while quiescent neurons were *less* excitable than those in shams (Fig. 4).

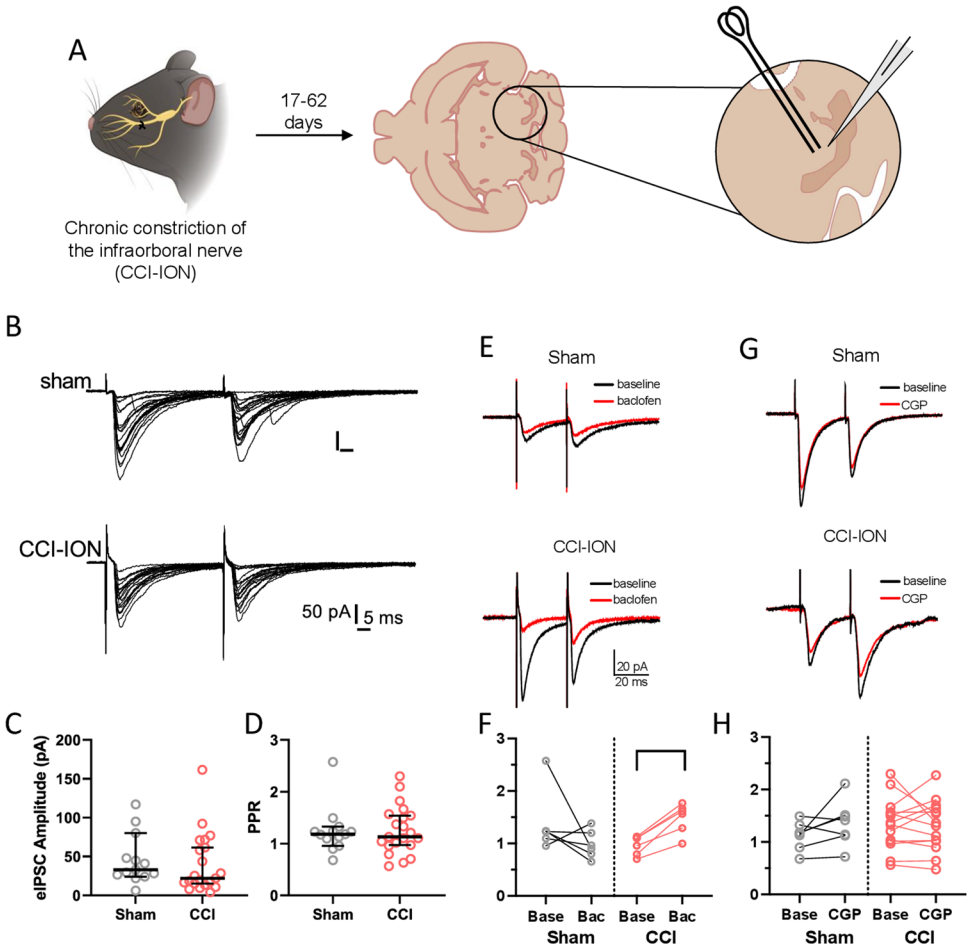

Figure 6. Phasic $GABA_B$ inhibition of inhibitory afferents in PBN is enhanced after nerve injury. ***A***, Experimental schematic. ***B***, Samples of electrically evoked IPSCs in a PBN neuron from a sham (top) and CCI (bottom) mouse. Each depicts an overlay of 20 responses to paired-pulse stimulation (50 ms interpulse interval). All traces have been baseline corrected. Neither the amplitude (***C***) or PPR (***D***) was affected by CCI. ***E***, Sample recordings from sham (top) and CCI neurons (bottom) before and after bath application of the $GABA_B$ agonist baclofen (1 μM, red trace). ***F***, As a population, baclofen had no effect on PPR in neurons from sham mice but significantly increased PPR in neurons from CCI-ION mice. In contrast, the $GABA_B$ antagonist CGP55845 (1 μM) had no effect on PPR from either group (***G,H***). Each trace in (***E***) and (***G***) are the average of 20 baseline-corrected individual trials, and the stimulus artifact has been truncated vertically for clarity. Wilcoxon matched-pairs test: $^*p < 0.05$.

To our knowledge, injury-induced hypoexcitability has yet to be described in PBN but are consistent with heterogeneity in injury-related changes in other brain regions, such as the amygdala (Li and Sheets, 2018; Wilson et al., 2019).

The projection patterns of hyper- and hypoexcitable PBN neurons will be important to determine as PBN pathways that mediate different aspects of pain behaviors have been identified (Chiang et al., 2020).

Differences between cuff and CCI-ION outcomes

In contrast to our data from the sciatic cuff model, there were no differences in intrinsic excitability of PBN neurons animals with CCI-ION. These disparate findings may arise from differences inherent to the trigeminal and spinal nociceptive pathways or differences in recording conditions.

Although both sciatic cuff and CCI-ION use peripheral nerve damage to model neuropathic pain, the models differ in important respects. In rodents, noxious stimuli applied to the face evoke a more robust and bilateral response in PBN than similar stimuli applied to the body (Hermanson and Blomqvist, 1997; Rodriguez et al., 2017). The organization of spinal trigeminal nucleus (SpV) into subnuclei, oralis (Vo), interpolaris (Vi), and caudalis (Vc), may contribute to this effect. Noxious trigeminal input not only activates second-order neurons in the subnucleus caudalis (SpVc), i.e., the medullary dorsal horn, but subsets of neurons at the Vi/Vc transition zone (Bereiter et al., 2000; Ikeda et al., 2003; Ren and Dubner, 2011). Similar to SpVc neurons, ViVc neurons project to PBN but show bilateral activation to noxious orofacial stimulation (Ikeda et al., 2003).

Also unique to the trigeminal pathway are subsets of peripheral trigeminal neurons that bypass the spinal trigeminal nucleus and project directly to PBN (Rodriguez et al., 2017; Uddin et al., 2021). In mice, activation of these neurons elicits aversive behaviors (Rodriguez et al., 2017). This direct pathway further suggests that trigeminal and spinal nociceptive signals are processed differently by central networks.

Another source of potential variability in this study are the differences in recording conditions: 32–34°C for recordings from coronal sections from sciatic cuff mice versus room temperature (~24°C) and horizontal sections for CCI-ION recordings. We controlled for these differences by performing separate comparisons on data from each model. The lack of significant changes in intrinsic properties of PBN neurons in either model suggests that these metrics remain relatively unaltered following peripheral nerve injury. Lastly, sex-based differences in the response of PBN neurons to injury may also be a factor, since our cuff/sham data are from male mice while our data from CCI-ION are from a mix of male and female mice. Future experiments will examine these possibilities more closely.

The role of $GABA_B$ in PBN injury-induced plasticity

We did not observe significant injury-induced changes in the capacitance, input resistance, rheobase, or single action potential waveforms of lPBN neurons, suggesting that alterations in intrinsic membrane properties are not a major contributor to the observed differences in excitability. Prior studies, however, suggest that deficits in GABAergic signaling may have a greater impact on PBN excitability. Long-range GABAergic inputs from the CeA are suppressed in the CCI-ION model and optogenetic activation of these inputs reverses pain behaviors (Raver et al., 2020). Similarly, optogenetic inhibition of GABAergic neurons in the PBN can induce pain-like behavior in uninjured mice (Sun et al., 2020). Our results suggest that changes in $GABA_B$ autoinhibition may underlie these phenomena and make a larger contribution to increased PBN excitability. We found no differences in the amplitudes of electrically eIPSCs in PBN slices from sham and CCI-ION mice. There were also no differences in IPSC PPR between the two groups, suggesting that the probability of synaptic release at inhibitory synapses is not affected by injury. However, the addition of a low concentration of baclofen, a $GABA_B$ agonist, selectively increased the IPSC PPR in slices from CCI-ION mice (Fig. 6), suggesting that autoinhibition of GABAergic afferents is enhanced following nerve injury. This decrease in inhibitory drive to PBN, along with potential changes in excitatory synaptic transmission, may contribute to the hyperexcitability observed in these neurons in models of chronic pain.

PBN circuitry: outputs and intra-PBN signaling

We did not determine which specific PBN pathways are impacted by peripheral nerve injury and how these changes may interact to promote the hyperexcitability phenotype associated with neuropathic pain. This will be important to address in future studies since specific PBN outputs have been linked to particular aspects of aversion and nocifensive responses. For example, the excitability of PBN neurons that project to the CeA have been causally linked to affective pain behaviors (Chen et al., 2018; Chiang et al., 2020; Liu et al., 2022; Allen et al., 2023; Torres-Rodriguez et al., 2023) despite showing no changes in intrinsic properties (Torres-Rodriguez et al., 2023). In this case, a reduction of the strength of inhibitory inputs to PBN neurons appears to play a more central role (Raver et al., 2020). It remains to be determined whether similar changes (or the lack thereof) occur in other PBN pathways linked to affective aspects pain behaviors, including projections to the bed nucleus of the stria terminalis (Chen et al., 2018; Chiang et al., 2020), ventral tegmental area (Yang et al., 2021), reticular formation (Barik et al., 2018), periaqueductal gray (Chiang et al., 2020), substantia innominata (Bowen et al., 2020), and various hypothalamic (Bowen et al., 2020; Chiang et al., 2020) and thalamic nuclei (Bowen et al., 2020; Deng et al., 2020). One possible consequence of increased lPBN excitability could be increased output onto these targets, leading to increased nociception and nocifensive behaviors. Shifts onto higher firing frequencies might also have the consequence of promoting release of neuropeptide-containing dense core vesicles (Park and Kim, 2009). Calcitonin gene–related peptide (CGRP) in particular plays an important role in injury-induced plasticity in the PBN→CeA pathway (Han et al., 2010, 2005; Okutsu et al., 2017; Shinohara et al., 2017; Allen et al., 2023), and increased CGRP release has been shown to have stark consequences for CeA activity (Han et al., 2005; Shinohara et al., 2017; Okutsu et al., 2017; Presto and Neugebauer, 2022; Allen et al., 2023).

Hyperexcitability of PBN neurons is frequently observed in models of chronic pain and associated with exaggerated pain behaviors. Our study finds that changes in the intrinsic properties of PBN neurons are unlikely to be the primary mechanism underlying this hyperexcitability. Although subsets of RS PBN neurons show injury-induced changes in excitability, our data suggest enhanced suppression of inhibitory afferents by $GABA_B$ receptors make a larger contribution to the amplified responses of PBN neurons in animal models of chronic pain.

References

Al-Khater KM, Todd AJ (2009) Collateral projections of neurons in laminae I, III, and IV of rat spinal cord to thalamus, periaqueductal gray matter, and lateral parabrachial area. J Comp Neurol 515:629–646.

Allen HN, Chaudhry S, Hong VM, Lewter LA, Sinha GP, Carrasquillo Y, Taylor BK, Kolber BJ (2023) A parabrachial-to-amygdala circuit that determines hemispheric lateralization of somatosensory processing. Biol Psychiatry 93:370–381.

Barik A, Thompson JH, Seltzer M, Ghitani N, Chesler AT (2018) A brainstem-spinal circuit controlling nocifensive behavior. Neuron 100:1491–1503.e3.

Barik A, Sathyamurthy A, Thompson J, Seltzer M, Levine A, Chesler A (2021) A spinoparabrachial circuit defined by Tacr1 expression drives pain. Elife 10:e61135.

Bellavance LL, Beitz AJ (1996) Alteredc-fos expression in the parabrachial nucleus in a rodent model of CFA-induced peripheral inflammation. J Comp Neurol 366:431–447.

Benbouzid M, Pallage V, Rajalu M, Waltisperger E, Doridot S, Poisbeau P, Freund-Mercier MJ, Barrot M (2008) Sciatic nerve cuffing in mice: a model of sustained neuropathic pain. Eur J Pain 12:591–599.

Bereiter DA, Hirata H, Hu JW (2000) Trigeminal subnucleus caudalis: beyond homologies with the spinal dorsal horn. Pain 88:221–224.
Bernard JF, Besson JM (1990) The spino(trigemino)pontoamygdaloid pathway: electrophysiological evidence for an involvement in pain processes. J Neurophysiol 63:473–490.
Bernard JF, Peschanski M, Besson JM (1989) A possible spino (trigemino)-ponto-amygdaloid pathway for pain. Neurosci Lett 100:83–88.
Bernard JF, Huang GF, Besson JM (1994) The parabrachial area: electrophysiological evidence for an involvement in visceral nociceptive processes. J Neurophysiol 71:1646–1660.
Bester H, Matsumoto N, Besson J-M, Bernard J-F (1997) Further evidence for the involvement of the spinoparabrachial pathway in nociceptive processes: a c-Fos study in the rat. J Comp Neurol 383:439–458.
Bester H, Beggs S, Woolf CJ (2000) Changes in tactile stimuli-induced behavior and c-Fos expression in the superficial dorsal horn and in parabrachial nuclei after sciatic nerve crush. J Comp Neurol 428:45–61.
Bourgeais L, Monconduit L, Villanueva L, Bernard J-F (2001) Parabrachial internal lateral neurons convey nociceptive messages from the deep laminas of the dorsal horn to the intralaminar thalamus. J Neurosci 21:2159–2165.
Bowen AJ, Chen JY, Huang YW, Baertsch NA, Park S, Palmiter RD (2020) Dissociable control of unconditioned responses and associative fear learning by parabrachial CGRP neurons. Elife 9: e59799.
Campos CA, Bowen AJ, Roman CW, Palmiter RD (2018) Encoding of danger by parabrachial CGRP neurons. Nature 555:617–622.
Cechetto DF, Standaert DG, Saper CB (1985) Spinal and trigeminal dorsal horn projections to the parabrachial nucleus in the rat. J Comp Neurol 240:153–160.
Chen JY, Campos CA, Jarvie BC, Palmiter RD (2018) Parabrachial CGRP neurons establish and sustain aversive taste memories. Neuron 100:891–899.e5.
Chiang MC, Bowen A, Schier LA, Tupone D, Uddin O, Heinricher MM (2019) Parabrachial complex: a hub for pain and aversion. J Neurosci 39:8225–8230.
Chiang MC, Nguyen EK, Canto-Bustos M, Papale AE, Oswald A-MM, Ross SE (2020) Divergent neural pathways emanating from the lateral parabrachial nucleus mediate distinct components of the pain response. Neuron 106:927–939.e5.
Choi S, et al. (2020) Parallel ascending spinal pathways for affective touch and pain. Nature 587:258–263.
Craig AD (1995) Distribution of brainstem projections from spinal lamina I neurons in the cat and the monkey. J Comp Neurol 361:225–248.
Cramer N, Silva-Cardoso G, Masri R, Keller A (2021) Control of synaptic transmission and neuronal excitability in the parabrachial nucleus. Neurobiol Pain 9:100057.
Deng J, et al. (2020) The parabrachial nucleus directly channels spinal nociceptive signals to the intralaminar thalamic nuclei, but not the amygdala. Neuron 107:909–923.e6.
Dutschmann M, Herbert H (1997) Fos expression in the rat parabrachial and Kölliker-Fuse nuclei after electrical stimulation of the trigeminal ethmoidal nerve and water stimulation of the nasal mucosa. Exp Brain Res 117:97–110.
Han JS, Li W, Neugebauer V (2005) Critical role of calcitonin gene-related peptide 1 receptors in the amygdala in synaptic plasticity and pain behavior. J Neurosci 25:10717–10728.
Han JS, Adwanikar H, Li Z, Ji G, Neugebauer V (2010) Facilitation of synaptic transmission and pain responses by CGRP in the amygdala of normal rats. Mol Pain 6:10.
Hayward LF, Felder RB (1999) Electrophysiological properties of rat lateral parabrachial neurons in vitro. Am J Physiol 276:R696–R706.
Hermanson O, Blomqvist A (1996) Subnuclear localization of FOS-like immunoreactivity in the rat parabrachial nucleus after nociceptive stimulation. J Comp Neurol 368:45–56.
Hermanson O, Blomqvist A (1997) Subnuclear localization of FOS-like immunoreactivity in the parabrachial nucleus after orofacial nociceptive stimulation of the awake rat. J Comp Neurol 387:114–123.
Hogri R, Teuchmann HL, Heinke B, Holzinger R, Trofimova L, Sandkühler J (2022) GABAergic CaMKIIα+ amygdala output attenuates pain and modulates emotional-motivational behavior via parabrachial inhibition. J Neurosci 42:5373–5388.
Ikeda T, Terayama R, Jue S-S, Sugiyo S, Dubner R, Ren K (2003) Differential rostral projections of caudal brainstem neurons receiving trigeminal input after masseter inflammation. J Comp Neurol 465:220–233.
Jergova S, Kolesar D, Cizkova D (2008) Expression of c-Fos in the parabrachial nucleus following peripheral nerve injury in rats. Eur J Pain 12:172–179.
Karthik S, et al. (2022) Molecular ontology of the parabrachial nucleus. J Comp Neurol 530:1658–1699.
Kim J, Alger BE (2001) Random response fluctuations lead to spurious paired-pulse facilitation. J Neurosci 21:9608–9618.
Kobashi M, Bradley RM (1998) Differences in the intrinsic membrane characteristics of parabrachial nucleus neurons processing gustatory and visceral information. Brain Res 781:218–226.
Li J, Sheets PL (2018) The central amygdala to periaqueductal gray pathway comprises intrinsically distinct neurons differentially affected in a model of inflammatory pain. J Physiol 596:6289–6305.
Li L, Ding J, Ren Z, Han Q, Hu G, Xiao M (2006) Expression and colocalization of NADPH-diaphorase and Fos in the subnuclei of the parabrachial nucleus in rats following visceral noxious stimulation. Brain Res 1114:41–52.
Liu S, Ye M, Pao GM, Song SM, Jhang J, Jiang H, Kim J-H, Kang SJ, Kim D-I, Han S (2022) Divergent brainstem opioidergic pathways that coordinate breathing with pain and emotions. Neuron 110:857–873.e9.
Matsumoto N, Bester H, Menendez L, Besson JM, Bernard JF (1996) Changes in the responsiveness of parabrachial neurons in the arthritic rat: an electrophysiological study. J Neurophysiol 76:4113–4126.
Nagase M, Mikami K, Watabe AM (2019) Parabrachial-to-amygdala control of aversive learning. Curr Opin Behav Sci 26:18–24.
Okutsu Y, Takahashi Y, Nagase M, Shinohara K, Ikeda R, Kato F (2017) Potentiation of NMDA receptor-mediated synaptic transmission at the parabrachial-central amygdala synapses by CGRP in mice. Mol Pain 13:174480691770920.
Palmiter RD (2018) The parabrachial nucleus: CGRP neurons function as a general alarm. Trends Neurosci 41:280–293.
Park Y, Kim K-T (2009) Short-term plasticity of small synaptic vesicle (SSV) and large dense-core vesicle (LDCV) exocytosis. Cell Signal 21:1465–1470.
Pauli JL, Chen JY, Basiri ML, Park S, Carter ME, Sanz E, McKnight GS, Stuber GD, Palmiter RD (2022) Molecular and anatomical characterization of parabrachial neurons and their axonal projections. Elife 11:e81868.
Presto P, Neugebauer V (2022) Sex differences in CGRP regulation and function in the amygdala in a rat model of neuropathic pain. Front Mol Neurosci 15:928587.
Qi L, Lin S-H, Ma Q (2022) Spinal VGLUT3 lineage neurons drive visceral mechanical allodynia but not sensitized visceromotor reflexes. Neuron 111:669–681.e5.
Raver C, Uddin O, Ji Y, Li Y, Cramer N, Jenne C, Morales M, Masri R, Keller A (2020) An amygdalo-parabrachial pathway regulates pain perception and chronic pain. J Neurosci 40:3424–3442.
Ren K, Dubner R (2011) The role of trigeminal interpolaris-caudalis transition zone in persistent orofacial pain. Int Rev Neurobiol 97:207–225.
Rodriguez E, et al. (2017) A craniofacial-specific monosynaptic circuit enables heightened affective pain. Nat Neurosci 20:1734–1743.
Sanabria ER, Wozniak KM, Slusher BS, Keller A (2004) GCP II (NAALADase) inhibition suppresses mossy fiber-CA3 synaptic neurotransmission by a presynaptic mechanism. J Neurophysiol 91:182–193.

Shinohara K, Watabe AM, Nagase M, Okutsu Y, Takahashi Y, Kurihara H, Kato F (2017) Essential role of endogenous calcitonin gene-related peptide in pain-associated plasticity in the central amygdala. Eur J Neurosci 46:2149–2160.

Sun L, et al. (2020) Parabrachial nucleus circuit governs neuropathic pain-like behavior. Nat Commun 11:5974.

Teuchmann HL, Hogri R, Heinke B, Sandkühler J (2022) Anti-nociceptive and anti-aversive drugs differentially modulate distinct inputs to the rat lateral parabrachial nucleus. J Pain 23:1410–1426.

Torres-Rodriguez JM, et al. (2023) The parabrachial to central amygdala pathway is critical to injury-induced pain sensitization in mice. Neuropsychopharmacology. 49:508-520.

Torruella-Suárez ML, et al. (2020) Manipulations of central amygdala neurotensin neurons alter the consumption of ethanol and sweet fluids in mice. J Neurosci 40:632–647.

Uddin O, Studlack P, Akintola T, Raver C, Castro A, Masri R, Keller A (2018) Amplified parabrachial nucleus activity in a rat model of trigeminal neuropathic pain. Neurobiol Pain 3:22–30.

Uddin O, Anderson M, Smith J, Masri R, Keller A (2021) Parabrachial complex processes dura inputs through a direct trigeminal ganglion-to-parabrachial connection. Neurobiol Pain 9:100060.

Wilson TD, Valdivia S, Khan A, Ahn H-S, Adke AP, Gonzalez SM, Sugimura YK, Carrasquillo Y (2019) Dual and opposing functions of the central amygdala in the modulation of pain. Cell Rep 29:332–346.e5.

Yang H, de Jong JW, Cerniauskas I, Peck JR, Lim BK, Gong H, Fields HL, Lammel S (2021) Pain modulates dopamine neurons via a spinal–parabrachial–mesencephalic circuit. Nat Neurosci 24:1402–1413.